Hindawi
Shock and Vibration
Volume 2019, Article ID 7481746, 17 pages
https://doi.org/10.1155/2019/7481746

Research Article

Phase Synchronization Control of Two Eccentric Rotors in the Vibration System with Asymmetric Structure Using Discrete-Time Sliding Mode Control

Xiaozhe Chen and Lingxuan Li

School of Control Engineering, Northeastern University at Qinhuangdao, Qinhuangdao 066004, China

Correspondence should be addressed to Lingxuan Li; lingxuan_li@163.com

Received 11 January 2019; Revised 25 April 2019; Accepted 14 May 2019; Published 10 June 2019

Academic Editor: José J. Rangel-Magdaleno

Control synchronization of two eccentric rotors (ERs) in the vibration system with the asymmetric structure is studied to make the vibration system obtain the maximum excited resultant force and the driven power. Because this vibration system is essentially an underactuated system, a decoupling strategy for the control goal of the same phase motion between two ERs is proposed to reduce the order of state equation of the vibration system. According to the master-slave control scheme, the complex control objects are converted into the velocity control of the master motor and the phase control of the slave motor. Considering the self-adjusting of the vibration system as interference, controllers of the velocity and the phase difference are designed by applying the discrete-time sliding mode control, which is proved by Lyapunov theory. A vibration machine is designed for evaluating the performance of the proposed controllers. Two control schemes are presented: controlling one motor and controlling two motors, and two group experiments are achieved to investigate the dynamic coupling characteristic of the vibration system in the state of control synchronization. The experimental results show that control synchronization is an effective and feasible technology to remove the limitation of vibration synchronization.

1. Introduction

Vibration machine is a new type of machine quickly developed in the twentieth century, which utilizes vibration principle to perform various processing tasks and has been widely used in various fields of industry [1]. They usually adopt an eccentric rotor (ER) as the excited source. By combining two ERs in different rotational directions and different installation positions, the vibration machine acquires the different resultant force and the motion trajectory to satisfy the processing requirements [2–4]. Hence, how to guarantee the synchronous motion between two ERs becomes a research topic [5, 6]. In the early design of vibration machine, the method of forced synchronization, such as gear and belt, is the only way to achieve the synchronous motion of two ERs, which is actually a passive control.

Since Blekhman studied self-synchronization of two ERs in the vibration system using the small parameter of Poincare-Lyapunov [5], more and more scholars are attracted to study self-synchronization from every respect [7–14]. Self-synchronization of the vibration system (also called vibration synchronization) is of great significance in engineering and technology fields because it replaces the technology of forced synchronization as the design technology of 2nd generation vibration machine. The technology of vibration synchronization utilizes the dynamic coupling characteristic of the vibration system to guarantee the synchronous motion of two ERs, which reflects the vibration system has the ability of the self-adjusting [2]. Hence, vibration synchronization is essentially semiactive control of applying the self-adjusting of the vibration system.

In some vibration machines, such as vibration mill, eccentric excitation caused by the asymmetric structure is needed to prevent the same amplitude at all positions of the system [1]. Although vibration synchronization utilizes the dynamic coupling characteristic of the vibration system to guarantee the synchronization of two ERs, the phase difference between two ERs is not usually equal to zero because of the stability limit of the system [3, 15, 16]. Because the stability of the vibration system depends on its structure parameters when two are ERs are operating with the asymmetric structure, the phase difference between two ERs is not equal to zero, which results in the smaller resultant force [3]. It is remarked that only when two ERs are operating in the same phase, their resultant force is the maximum value. To obtain the maximum excited resultant force and the driven power, the viewpoint of introducing control theory into the design of a vibration machine (also called control synchronization) is proposed [5]. Therefore, the technology of active control is the development trend of 3rd vibration machine.

Because the vibration system has the ability of the self-adjusting, the control synchronization of two ERs in the vibration system is different from that of two motors in other mechanical systems [17]. Now, there are several control strategies for multimotors in the general system, e.g., the master-slave control [18], the cross-coupling control [19], the virtual shaft control [20], and the ring coupling control [21]. In engineering, the master-slave control is the most direct and effective method compared with other methods. Based on the master-slave control strategy, several scholars studied control synchronization of two ERs in the vibration system with symmetric structure. Kong [17] applied slide mode control (SMC) to study control synchronization of the vibration system with symmetrical structure. Tomchina [22] adopted PI control to investigate control synchronization of the vibration system with one degree of freedom. Jia [23] proposed a fuzzy PID method to study multiple-frequency synchronization of the vibration system with symmetrical structure. Fradkov [24] applied PI control to study the multiple-frequency control synchronization for 3-rotor vibration unit with varying payload. Miklos [11] applied PI control to study control synchronization of a dual-rotors system. To some extent, these results promote the development of control synchronization of the vibration system with symmetric structure. However, some results still need to be proved by experiment, because control methods of continuous-time cannot be directly applied in a microprocessor to control practical systems.

Considering the engineering requirement, this paper studied control synchronization of two ERs in the vibration system with the asymmetric structure. For this type of nonlinear system, this paper uses discrete-time sliding mode control (DSMC) to carry out the experimental research [25, 26]. To easily observe the dynamic coupling characteristic of the vibration system in the state of control synchronization, DC motor is adopted as the driven source. In the next section, the electromechanical mathematic model is presented. Next, controllers are designed. Additionally, an experimental system is introduced. Later, experimental results are achieved. Finally, conclusions are presented.

2. Dynamic Model of the Vibration System

The dynamic model, the vibration machine, the experimental system, and experimental flow are shown in Figure 1. Comparing Figures 1(a) and 1(b), the dynamic model of the vibration system mainly consists of a fixed base (Num 1), springs (Num 2), a rigid body (Num 3), and two ERs (Num 4). Additional details about the numbers are shown in Table 1. The springs connect the base with the rigid body. The mass center G of the vibration system translations is x and y, and angular rotation is ψ. Two ERs are direct-driven by DC motor in the clockwise direction, respectively. o_i are the rotational centers of ERs, r is the eccentric radius of two ERs, and φ_i denote ER rotates about its spin axis, $i = 1, 2$. Two vibration motors (two eccentric mass blocks are installed on both ends of the motor shaft) are not fixed symmetrically based on the Y-axis passing through the mass center of the system, and they are fixed to the left of the Y-axis. So, the system of Figure 1 is a type of the asymmetric structure because of external excitation from two ERs. Because the spring is made of high-carbon steel and is cylindrical, the spring stiffness can be approximately linear when the system works at the far resonance [1]. Selecting the x, y, ψ, φ_1, and φ_2 as the generalized coordinates and using Lagrange's equation, the electromechanical mathematic model of the vibration system is expressed as follows [16]:

$$\begin{aligned}
M\ddot{x} + f_x\dot{x} + k_x x &= \sum_{i=1}^{2} \sigma m_i r\left(\dot{\varphi}_i^2 \cos\varphi_i + \ddot{\varphi}_i \sin\varphi_i\right),\\
M\ddot{y} + f_y\dot{y} + k_y y &= \sum_{i=1}^{2} m_i r\left(\dot{\varphi}_i^2 \sin\varphi_i - \ddot{\varphi}_i \cos\varphi_i\right),\\
J_\psi\ddot{\psi} + f_\psi\dot{\psi} + k_\psi\psi &= \sum_{i} r m_i l_i\left[\dot{\varphi}_i^2 \sin\left(\varphi_i - \sigma\beta_i\right) - \ddot{\varphi}_i \cos\left(\varphi_i - \sigma\beta_i\right)\right],\\
J_i\ddot{\varphi}_i + f_i\dot{\varphi}_i &= T_{ei} - T_{Li},
\end{aligned} \tag{1}$$

where $T_{Li} = m_i r$ $[\ddot{y}\cos\varphi_i - \sigma\ddot{x}\sin\varphi_i + l_i\ddot{\psi}\cos(\varphi_i - \sigma\beta_i) + l_i\dot{\psi}^2\sin(\varphi_i - \sigma\beta_i)]$, $T_{ei} = K_{ti}I_i$ are the electromagnetic torques of two motors, $u_i = R_iI_i + K_{ei}\dot{\varphi}_i$ are the circuit equations of two motors, R_i are armature resistances, K_{ei} are electromotive force constants, K_{ti} are electromagnetic torque constants, u_i are the input voltages of DC motor, I_i are the input currents of DC motor, $J_i \approx m_i r^2$ are the moments of inertia of ERs, f_i are the damping coefficients of the axis of motor, and $i = 1, 2$; m is the mass of the rigid body, and m_i are the masses of ERs, $M = m + m_1 + m_2$, J_ψ is the moment of inertia of the vibration system; $\sigma = 1$ is the anticlockwise direction of ER, $\sigma = -1$ is the clockwise

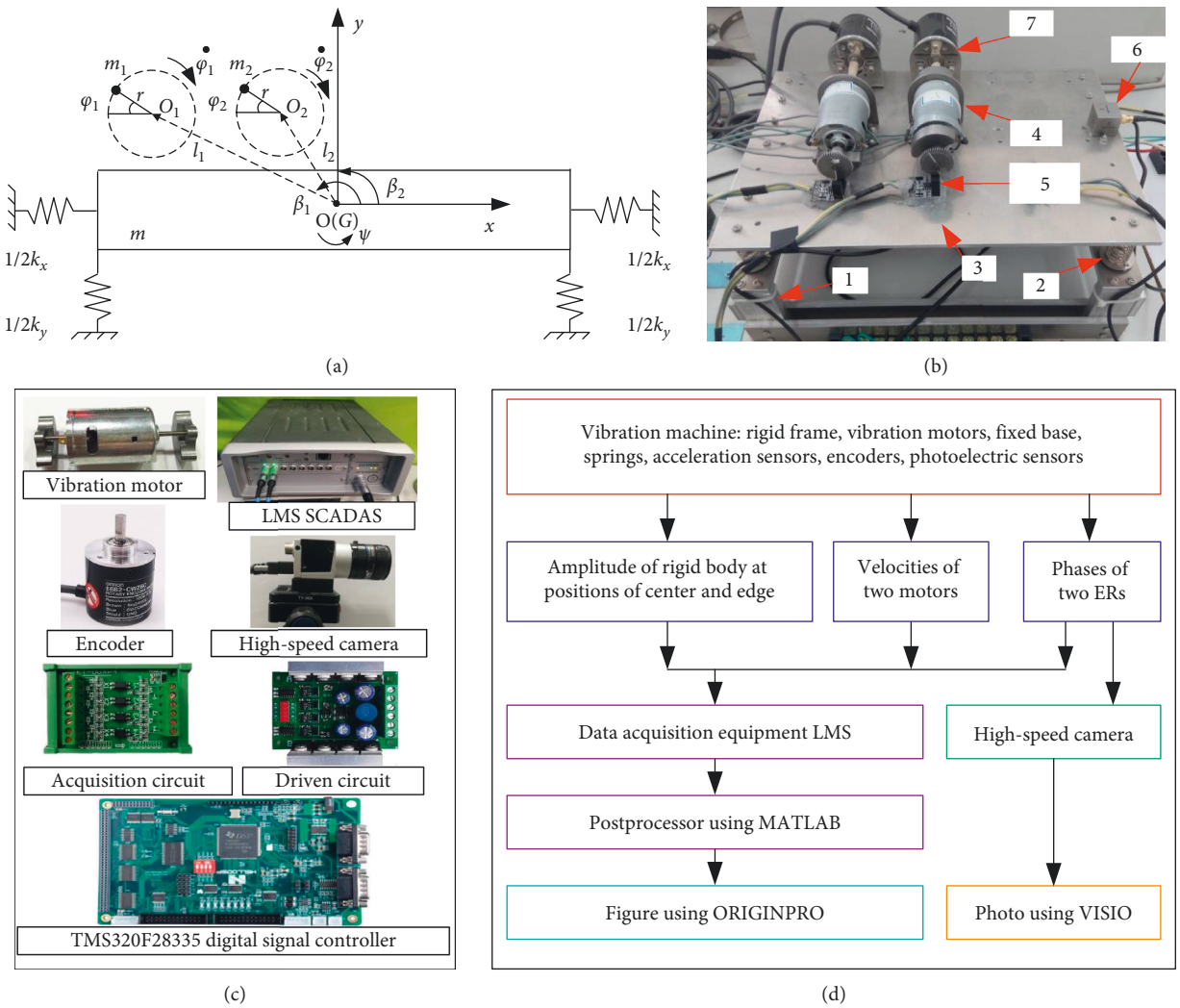

Figure 1: The vibration system driven by two ERs. (a) The dynamic model. (b) The vibration machine. (c) The experimental equipment. (d) The experimental flow.

Table 1: Code table.

Number	Designation	Application
1	Fixed base	Providing structural support
2	Spring	Connecting rigid body and fixed base
3	Rigid body	Using to install related devices
4	ER	As a source of motivation
5	Photoelectric sensor	Providing signal to acquisition instrument
6	Acceleration sensor	Providing signal to acquisition instrument
7	Encoder	Providing signal to controller

direction of ER; l_i are the distances between the rotational center o_i and the center of mass G, and β_i are the angles between line o_iG and x-axis, $i = 1, 2$; k_x, k_y, k_ψ are stiffness of springs and f_x, f_y, f_ψ are damping of springs; $(\dot{\bullet})$ and $(\ddot{\bullet})$denotes $d(\bullet)/dt$ and $d^2(\bullet)/dt^2$.

Since the excitation of ER is periodic, the responses of the steady state of the system are obtained as follows [16]:

$$x = \sum_{i=1}^{2} \frac{\sigma r m_0 \dot{\varphi}_i^2 \cos(\varphi_i - \gamma_{xi})}{k_x - M\dot{\varphi}_i^2},$$

$$y = \sum_{i=1}^{2} \frac{r m_0 \dot{\varphi}_i^2 \sin(\varphi_i - \gamma_{yi})}{k_y - M\dot{\varphi}_i^2}, \tag{2}$$

$$\psi = \sum_{i=1}^{2} \frac{r m_0 \dot{\varphi}_i^2 l_i \sin(\varphi_i - \sigma\beta_i - \gamma_{\psi i})}{k_\psi - J_\psi \dot{\varphi}_i^2},$$

where $m_1 = m_2 = m_0$, $\gamma_{xi} = \arctan[f_x\dot{\varphi}_i/(k_x - M\dot{\varphi}_i^2)]$, $\gamma_{yi} = \arctan[f_y\dot{\varphi}_i/(k_y - M\dot{\varphi}_i^2)]$, $\gamma_{\psi i} = \arctan[f_\psi\dot{\varphi}_i/(k_\psi - J_\psi\dot{\varphi}_i^2)]$, and $i = 1, 2$.

3. DSMC Controllers and Stability Analysis

Combining equation (1) with equation (2), the inputs of the vibration system are T_{ei} and the outputs of that are x, y, ψ, φ_1, and φ_2, which explains that the vibration system driven by two ERs is a typical underactuated system. Although this

type of underactuated system usually adopts the backstepping control, it is not necessary for the vibration system of this paper. The control goal is achieving the maximum resultant force according to the processing requirements. Hence, the control goal is transformed into the same phase motion of ERs based on the force analysis of the vibration system. Furthermore, ER is direct-driven by the motor. So, the complex control is converted into controlling velocities and phases of motors.

Obviously, the motions of two motors are not unrelated according to T_{Li} of equation (1), and they operate in a coupling state. As shown in Figure 2, it explains the dynamic coupling characteristic of the vibration system, also called the self-adjusting; meanwhile, it illuminates that control of two motors in the vibration system is different from that in the general system [18, 27, 28]. The self-adjusting process is that the motor directly drives ER to excite the vibration system by rotational motion φ_1 and φ_2, while the vibration system changes the load torque of motor by motion itself in x, y, and ψ [2, 29]. In this way, the vibration system reaches a steady state. However, if the vibration system is the asymmetric structural, the phases of two ERs are usually different under the function of the self-adjusting [3, 4, 29]. Hence, in order to design the controller of the motor, how to decouple the motion equation of the motor becomes the control key.

It should be remarked that this self-adjusting is still limited even if it is strong. Because the structure parameters are constant, equation (2) is only the function of variable φ_1 and φ_2 with time. Furthermore, T_{Li} of equation (1) are also bounded, which illuminates that the self-adjusting also has bounded. Hence, the self-adjusting can be considered as an internal disturbance. Based on the above analysis, the control object transforms into a single input and single output model with disturbance.

According to the master-slave control scheme, the active control of two motors is divided into two parts: velocity-loop and phase-loop in Figure 2. Firstly, velocity-loop is used to control the excited frequency. Secondly, phase-loop is used to guarantee the same phase motion for the maximum resultant force. If there is no velocity control or the excited frequency requirement, only controlling one motor can ensure the same phase motion of two motors, which saves costs in engineering. It has to be mentioned that the phase difference should be chosen as the control object for phase-loop because the phase of motor keeps increasing at rotational motion. Hence, the master motor is used only for open-loop and closed-loop velocity control, and the slave motor is used for closed-loop phase tracking control, as shown in Figure 2.

Because DC motor has the weak mechanical characteristics, it is easy to observe the change of the velocity with the change of the load torque. So, DC motor is adopted as the driven source. In engineering, the controller is divided into two parts: the algorithm controller and the executive controller. Of course, the algorithm controller is a velocity controller or a phase controller. At present, the pulse width modulation (PWM) of voltage is the most common technique of motor control in engineering. Hence, we adopt the PWM calculator as an executive controller. Considering the self-adjusting is a fast variable with time according to Figure 2, SMC is more suitable for this kind of control with internal parameter perturbations and disturbances [25, 26].

The mathematical model of DC motor is usually expressed by a second-order system as follows [30]:

$$\begin{cases} \dot{\varphi}_i = \omega_i, \\ \dot{\omega}_i = -\dfrac{f_i R_i + K_{ti} K_{ei}}{J_i R_i}\omega_i + \dfrac{K_{ti}}{J_i R_i} u_i - \dfrac{1}{J_i} T_{Li}. \end{cases} \tag{3}$$

Selecting the velocity of the master motor and the phase difference between two ERs as the state variables, $z_1 = \dot{\varphi}_1$, and $z_2 = \dot{\varphi}_1 - \dot{\varphi}_2 = 2\dot{\alpha}$, the state equations of the master motor and the slave motor are rearranged, respectively, as

$$\dot{z}_1 = a_1 z_1 + b_1 u_1 + W_1, \tag{4}$$

$$\dot{z}_2 = a_2 z_2 + b_1 u_1 - b_2 u_2 + (a_1 - a_2) z_1 + W_1 - W_2, \tag{5}$$

where $a_i = -(f_i R_i + K_{ti} K_{ei}/J_i R_i)$, $b_i = (K_{ti}/J_i R_i)$, $W_i = \Delta a_i + \Delta b_i - T_{Li}/J_i$, and $i = 1, 2$. a_i and b_i denote the nominal value of parameters, Δa_i and Δb_i denote the perturbation of parameters, W_i denote the lump uncertainties from the self-adjusting of the vibration system, and it is bounded because T_{Li} are also bounded.

3.1. Velocity Controller of the Master Motor. The setting value ω_t is selected as the control goal of the angular velocity of the master motor, and the tracking error is expressed as

$$e_1 = z_1 - \omega_t. \tag{6}$$

When this task implements SMC in a practical system, DSMC with a digital microcontroller must be considered. Since the sampling interval T_s of this work is close to 10 kHz, equation (4) can be transformed to the discrete state equation with the sampling interval T_s as [25, 26]

$$z_1(k+1) = g_1 z_1(k) + h_1 u_1(k) + L_1, \tag{7}$$

where $g_1 = T_s a_1 + 1$, $h_1 = T_s b_1$, $L_1 = T_s W_1(k)$, and $k = 0, 1, 2, 3, \cdots$ denote the discrete-time function.

The control type of equation (4) is the tracking problem because of the control goal of the master motor. Employing the difference approach to this discrete-time system, the sliding mode existence condition is as follows:

$$\begin{aligned} s_1(k) &= c_1 e(k) + \frac{[e(k) - e(k-1)]}{T_s} \\ &= \frac{[(c_1 T_s + 1) e(k) - e(k-1)]}{T_s}, \end{aligned} \tag{8}$$

where c_1 must satisfy Hurwitz, $c_1 > 0$ [31]; $e(k) = z_1(k) - \omega_t(k)$.

By analogy with continuous-time systems, the equivalent control can yield motion in the manifold $s_1 = 0$. So the ideal quasi-sliding mode satisfies $s_1(k+1) = s_1(k)$. Ignoring the unknown term L_1, an equivalent control is given by

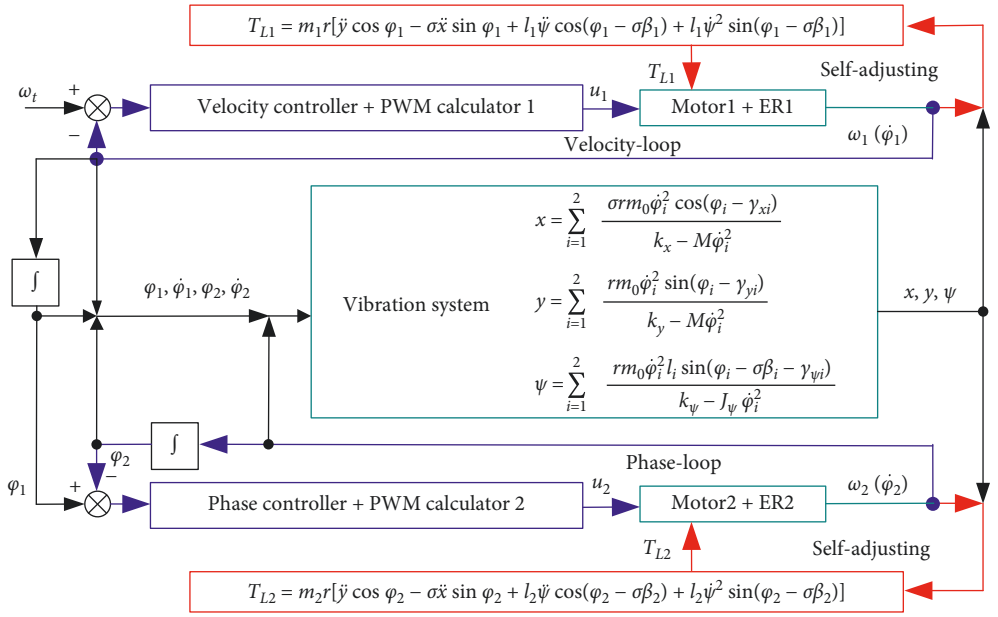

Figure 2: The control synchronization scheme of two ERs.

$$u_{\mathrm{eq1}}(k) = \frac{[c_1\omega_t(k+1) - c_1\omega_t(k) - \sigma_1 z_1(k) + \sigma_1 z_1(k-1)]}{(b_1 T_s)}, \tag{9}$$

where

$$\begin{aligned} \sigma_1 &= a_1 + c_1, \\ \omega_t(k+1) &= 2\omega_t(k) - \omega_t(k-1). \end{aligned} \tag{10}$$

Note that control resource of equation (9) is insufficient to stabilize the system, which is affected by the unknown term L_1. To hold on the reaching condition, the switching control is designed as

$$u_{\mathrm{sw1}}(k) = \frac{(D_1 + \varepsilon_1)}{b_1}, \tag{11}$$

where $D_1 > \max|W_1|$.

Hence, the control law of DSMC of the master motor is composed of equations (9) and (11) and is expressed as

$$u_1(k) = u_{\mathrm{eq1}}(k) + u_{\mathrm{sw1}}(k). \tag{12}$$

3.2. Phase Controller of the Slave Motor. The goal of control synchronization can be achieved by adjusting the phase difference between the master motor and the slave motor. When the phase difference equals to zero, the velocities of the master motor and the slave motor must be the same because of the rotational motion of the motor. So the phase-loop of the slave motor is enough for the control goal. Because the set value z_2 is essentially a difference, it is expected to be zero. Therefore, equation (5) is the error equation of the control error type. Same as equation (7), equation (5) can be transformed to the discrete state equation with the sampling interval T_s as

$$z_2(k+1) = g_2 z_2(k) + h_2 u_2(k) + L_2, \tag{13}$$

where

$$\begin{aligned} g_2 &= T_s a_2 + 1, \\ h_2 &= -T_s b_2, \\ L_2 &= T_s\left(b_1 u_1(k) + (a_1 - a_2) z_1(k) + W_1(k) - W_2(k)\right). \end{aligned} \tag{14}$$

Employing the difference approach to this discrete-time system, the sliding mode existence condition is as follows:

$$\begin{aligned} s_2(k) &= c_2 z_2(k) + \frac{[z_2(k) - z_2(k-1)]}{T_s} \\ &= \frac{[(c_2 T_s + 1) z_2(k) - z_2(k-1)]}{T_s}, \end{aligned} \tag{15}$$

where c_2 must satisfy Hurwitz, $c_2 > 0$ [31].

With the same dealing as equation (9), the equivalent control of DSMC for the slave motor is obtained as

$$u_{\mathrm{eq2}}(k) = -\frac{[\sigma_2 z_2(k) - \sigma_2 z_2(k-1) + b_1 T_s u_1(k) + (a_1 - a_2) T_s z_1(k)]}{(b_2 T_s)}, \tag{16}$$

where $\sigma_2 = a_2 + c_2$.

To eliminate the unknown term L_2, the switching control is designed as

$$u_{\mathrm{sw2}}(k) = \frac{(D_2 + \varepsilon_2)}{b_2}, \tag{17}$$

where $D_2 > \max|W_1 - W_2|$.

The control law of DSMC of the slave motor is expressed as

$$u_2(k) = u_{\mathrm{eq2}}(k) + u_{\mathrm{sw2}}(k). \tag{18}$$

3.3. Stability of Controllers. It is remarked that the stability and robustness of continuous-time SMC are guaranteed using Lyapunov stability theory and the formula of $s(t)\dot{s}(t) < 0$ [21]. Considering the smaller sample time ($0.1\,\text{ms} < T_s < 1\,\text{ms}$), the sliding condition and the convergence condition of DSMC is expressed as [26]

$$[s(k+1) - s(k)]\text{sgn}(s(k)) < 0, \tag{19}$$

$$[s(k+1) + s(k)]\text{sgn}(s(k)) > 0. \tag{20}$$

Theorem. *Robust stability to disturbance: for the two motors system, if the following conditions hold, then the control system described by equations (21) to (24) is stable:*

(i) $\varepsilon_1 > 0$, $\varepsilon_2 > 0$,

(ii) $D_1 > |W_1|$, $D_2 > |W_1 - W_2|$.

Proof. Substituting equations (8) and (12) into equations (19) and (20), the results of the velocity controller are obtained as follows:

$$\begin{aligned}[s_1(k+1) - s_1(k)]\text{sgn}(s_1(k)) &= T_s[W_1 - (D_1 + \varepsilon_1)\text{sgn}(s_1(k))] \\ &\quad \cdot \text{sgn}(s_1(k)) \\ &= T_s[W_1\text{sgn}(s_1(k)) - D_1 - \varepsilon_1] \\ &< -T_s\varepsilon_1 < 0,\end{aligned} \tag{21}$$

$$\begin{aligned}[s_1(k+1) + s_1(k)]\text{sgn}(s_1(k)) &= [s_1(k) - T_s(D_1 + \varepsilon_1) \\ &\quad \cdot \text{sgn}(s_1(k)) + T_sW_1] \\ &\quad \cdot \text{sgn}(s_1(k)) \\ &= |s(k)| - (D_1 + \varepsilon_1)T_s \\ &\quad + T_sW_1\text{sgn}(s_1(k)) > |s(k)| \\ &\quad - T_s(\varepsilon_1 + 2D_1) > 0.\end{aligned} \tag{22}$$

Equations (15) and (18) are also substituted into equations (19) and (20), and the result of the phase controller is

$$\begin{aligned}[s_2(k+1) - s_2(k)]\text{sgn}(s_2(k)) &= T_s[W_3 - (D_2 + \varepsilon_2) \\ &\quad \cdot \text{sgn}(s_2(k))]\text{sgn}(s_2(k)) \\ &= T_s[W_3\text{sgn}(s_2(k)) - D_2 - \varepsilon_2] \\ &< -T_s\varepsilon_2 < 0,\end{aligned} \tag{23}$$

$$\begin{aligned}[s_2(k+1) + s_2(k)]\text{sgn}(s_2(k)) &= [2s_2(k) - T_s(D_2 + \varepsilon_2) \\ &\quad \cdot \text{sgn}(s_2(k)) + T_sW_3] \\ &\quad \cdot \text{sgn}(s_2(k)) \\ &= |s_2(k)| - T_s(D_2 + \varepsilon_2) \\ &\quad + T_sW_3\text{sgn}(s_2(k)) > |s_2(k)| \\ &\quad - T_s(\varepsilon_2 + 2D_2) > 0.\end{aligned} \tag{24}$$

where $W_3 = W_1 - W_2$. In engineering, the vibration amplitude of most vibration machines is less than 5 mm and the vibration frequency of that is less than 50 Hz [3, 4]. So, if $T_s = 10\,\text{kHz}$, $T_s|W_1| \ll 1$ and $T_s|W_3| \ll 1$, $T_s|\varepsilon_1 + 2D_1| \ll 1$ and $T_s|\varepsilon_2 + 2D_2| \ll 1$. Hence, equations (22) and (24) are easily satisfied. Finally, the proof of the theorem is completed. □

4. Experimental System

The next section will evaluate the performance of the proposed controllers. In this section, some key operated steps will be introduced to make the experimental process easier to understand. The microprocessor TMS320F28335 made by TI corporation is selected as DSC (digital signal controller) to operate the control algorithm in this work, as shown in Figure 1(c). The incremental encoder E6B2-CWZ6C made by OMROM is selected to provide the signal of the motor for DSC, as shown in Figure 1(c), and its position is denoted by Num 7 in Figure 1(b). Other parts, such as the power circuit, driven circuit, and acquisition circuit, are needed for the experimental system. Because the motor directly drives ER, the velocity and the phase of ER are also the same as those of the motor, which is not emphasized in the following contents.

4.1. Control Scheme. As shown in Figure 3, the control logic based on microprocessor TMS320F28335 is presented. There are 12 steps for the control of two motors. The first three steps mainly configure the hardware system. The 4th step is used to define the function for controllers. The 5th step is used to assign values to parameters of controllers. We adopt the timer interrupt as the control base time in the 6th step. Once one timer interrupt is triggered, the corresponding control will be operated according to the control command in the 7th step, such as whether the master motor is closed-loop control or open-loop control in the 8th step. The 9th, 10th, and 11th are the important steps for DSMC controller in Section 3. The 9th step acquires signals from encoders and calculates the velocity and the phase difference. The 10th step calculates parameters of the velocity controller and the phase controller in Figure 2, such as $u_1(k)$ in equation (12). The 11th step converts the control input into PWM (pulse width modulation) by calculating the duty-cycle of the power voltage.

4.2. Calculating Velocity and Phase Difference. This section will propose a method for calculating the velocity and the phase difference of the 9th step to provide data for the 10th step in Figure 3. As shown in Figure 4, the calculation method based on microprocessor TMS320F28335 is presented.

Considering the conventional M/T method cannot calculate the exact value of the velocity for the vibration motor because of the vibration characteristic, the average approach of measuring multiple rotational periods of the motor is

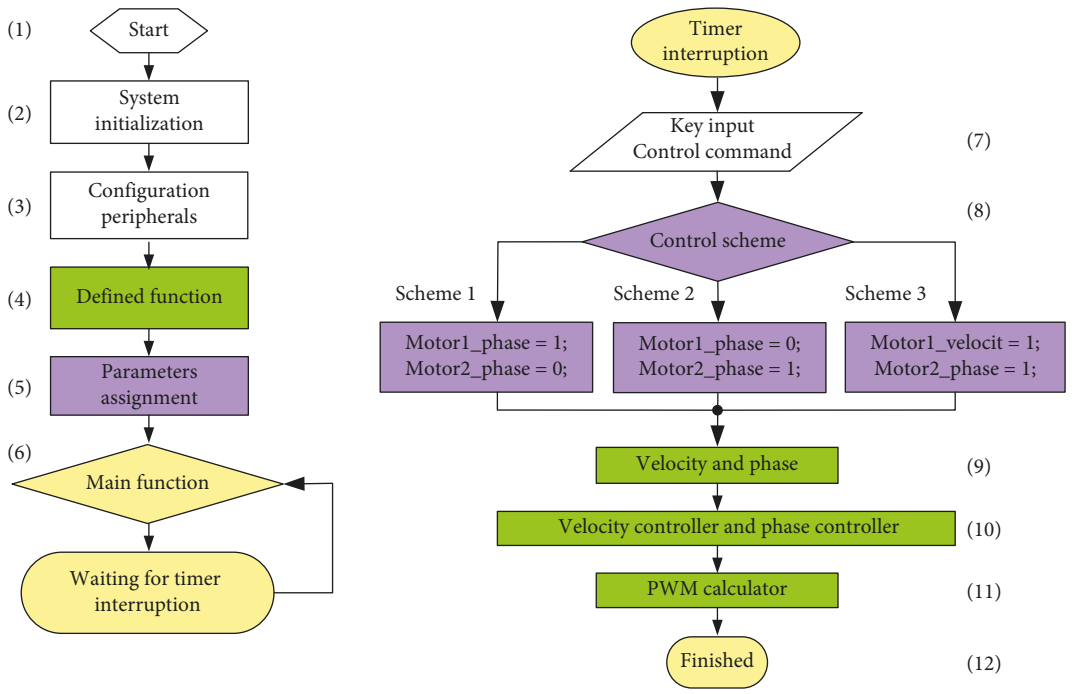

Figure 3: The schematic diagram of software.

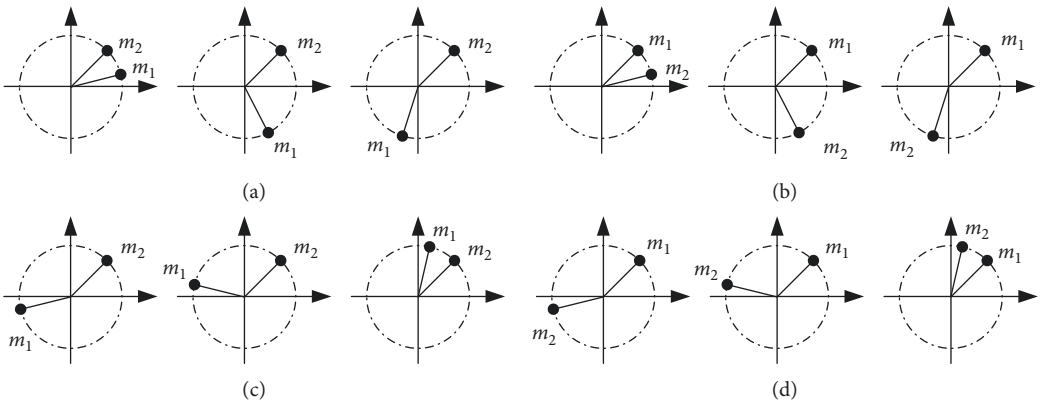

Figure 4: Change domain of the phases.

chosen to obtain a more accurate value of the motor velocity. Since overmuch period will lead to the loss of the real-time control, the calculating value is the average value of four rotational periods of the motor (the experimental velocity is about 1500 r/min). Other details are shown in the velocity part of Figure 5.

The phase difference cannot be calculated directly because the limit of QEP unit of TMS320F28335, and it requires a data conversion process. Meanwhile, the Z signal of an encoder is used to clear zero for the calculator function of QEP unit, which prevents the accumulation of measuring errors. Therefore, it is not correct to directly subtract the pulse number of two encoders because the calculator is affected by the cleaning process. In order to understand the process, multiple possible phase stages of two ERs are shown in Figure 4. Usually, the phase difference in the vibration system is expressed to be less than π, which is used to estimate whether ER is the leading phase or the lagging phase. When two ERs run in clockwise, the absolute values of the phase difference of Figures 4(a) and 4(b) are less than π. On the contrary, those of Figures 4(c) and 4(d) are greater than π. The values of the phase difference of Figure 4(a) are contrary to those of Figure 4(b). Particularly, it is necessary to determine whether there is a process of clearing zero. Specific methods are shown in the phase part of Figure 5.

4.3. Compiling DSMC. As shown in Figure 6, controllers of the velocity and the phase difference are compiled by using C programming language. All functions are done by calling pointers. Because of the practical system, the limitation adjustment must be considered to prevent inconvenient accidents. Other details are shown in Figure 6.

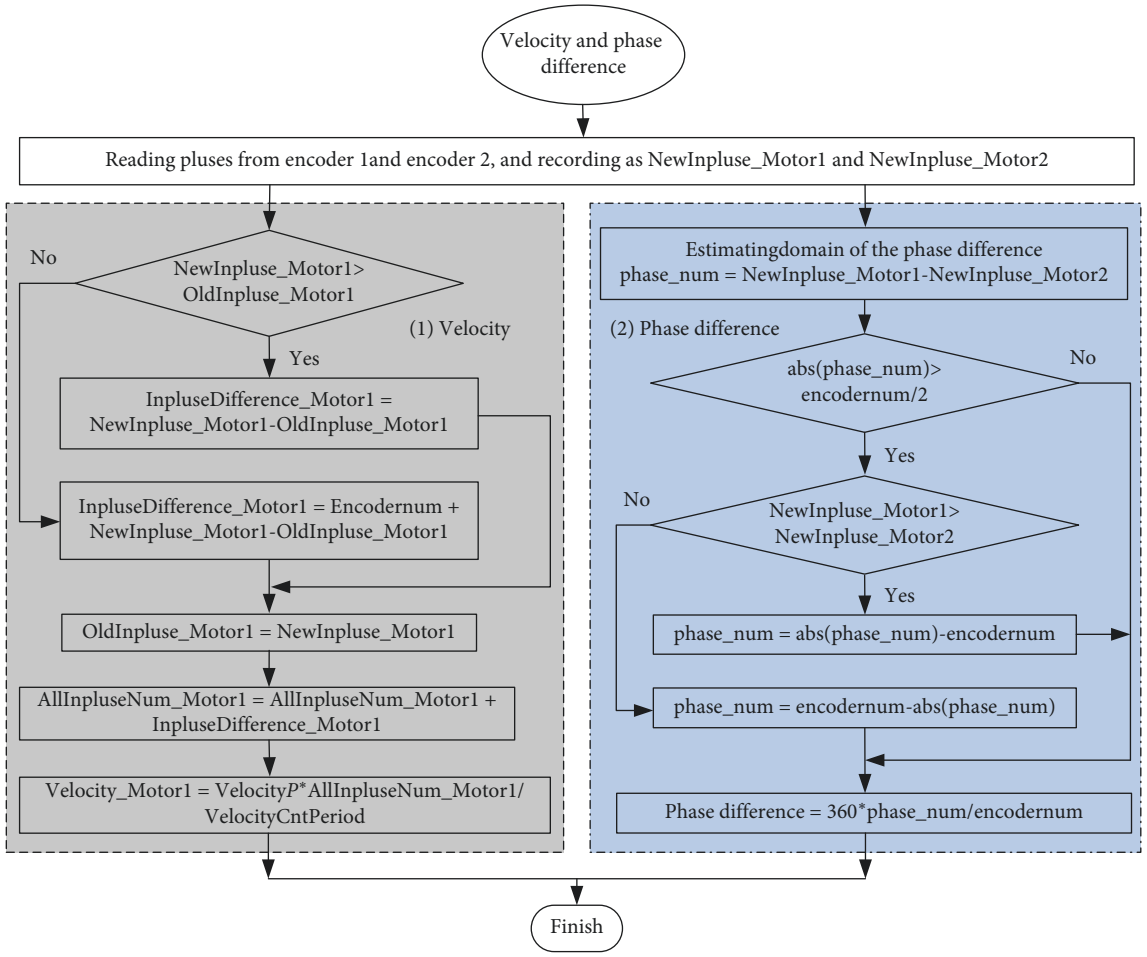

Figure 5: Calculation flow chart of velocity and the phase difference.

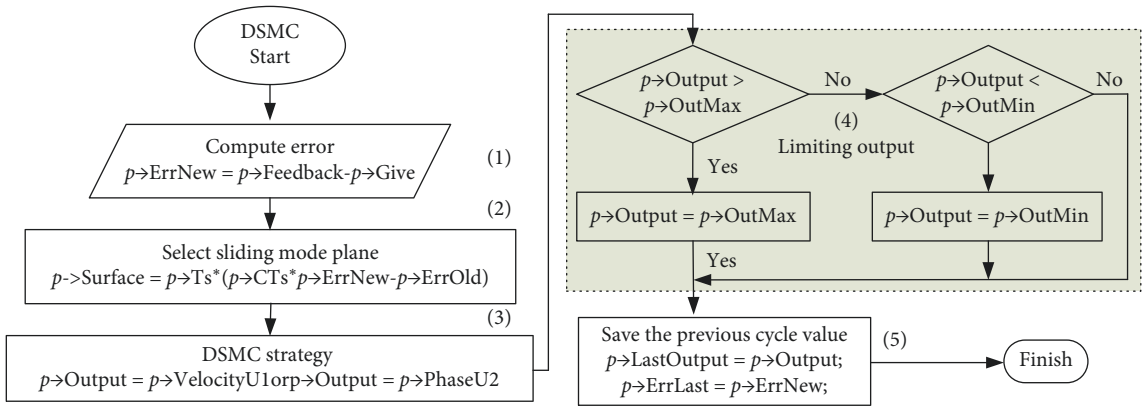

Figure 6: Calculation flow of DSMC.

5. Results and Discussion

Based on the master-slave control strategy and DSMC algorithmic proposed in Chapter 3, two group experiments are completed. By applying photoelectric sensors (Num 5 in Figure 1(b)) to record velocities of motors and acceleration sensors (Num 6 in Figure 1(b)) to measure amplitudes of two positions in the vertical and horizontal directions, these signal data are acquired by LMS SCADAS in Figure 1(c). Meanwhile, phases of ERs are captured by the high-speed camera in Figure 1(c). The acceleration signals are obtained from two positions of the mass center and the edge of the body. The parameters are as follows: $r = 10$ mm, $m_0 = 23$ g, $M = 1000$ g, $J_\psi = 60$ gm^2, $l_1 = 75$ mm, $l_2 = 26$ mm, $\beta_1 = 160^\circ$, $\beta_2 = 90^\circ$, $k_x \approx k_y \approx 6000$ N/m, $k_\psi \approx 1140$ N/m, $f_x \approx f_y \approx 34$ N/(m/s), $f_\psi \approx 27$ N·m/(rad/s), $f_1 \approx f_2 \approx 0.01$ N·m/(rad/s),

$R_i \approx 5.5\,\Omega$, $K_{ei} \approx 1.7$ Vs/rad, $K_{ti} \approx 25.4$ Nm/A, the rated velocity is 3000 r/min, and the rated voltage is 12V.

5.1. Vibration Synchronization and Control Synchronization. The comparison between vibration synchronization and control synchronization of two ERs with asymmetrical structure is shown in Figures 7–10. The experimental scheme is divided into three parts. First, two motors operate in the state of vibration synchronization. Second, the command of control synchronization is executed by controlling one motor. After 20 s, motor 1 adopting the open-loop control is the master motor and motor 2 is the slave motor adopting the closed-loop control of phase controller. After 40 s, the control strategy is exchanged.

To facilitate analysis and verify data, three group photos of two ERs with the asymmetric structure are firstly shown in Figures 7–9, respectively. Figure 7 shows the high-speed photos of two ERs with the anticlockwise rotational directions in the state of vibration synchronization, which is captured by the high-speed camera in 100 Hz. The phase difference is basically stable at −145°, and the phase of ER1 is lag of that of ER2, which reflects the function of the self-adjusting of the vibration system. On the contrary, Figure 8 shows the high-speed photos of two ERs with the clockwise rotational directions in the state of vibration synchronization. The phase difference is basically stable at −170°, and the phase of ER1 is still lag of that of ER2, which is different from that of the symmetrical structure. The two group photos of vibration synchronization reflect the inherent characteristics of the vibration system. Figure 9 shows the high-speed photos of two ERs with the clockwise rotational directions in the state of control synchronization. The eight photos of average time illuminate that the phase difference is approximately equal to 0°. Next, the data analysis of two ERs with the clockwise rotational directions in the state of vibration synchronization and control synchronization will be listed.

Figure 10 shows the curves of two ERs rotating in clockwise direction including velocity, phase difference, and amplitudes. In order to easily observe the motion states of the vibration system from start to steady state, the data time is delayed for a few seconds during the data processing, which is not explained below.

Figure 10(a) shows the velocity curves of two motors in the three stages of vibration synchronization and control synchronization. Once two motors obtain power supply, they rapidly reach the steady-state velocities, which is different from the characteristics of AC motor [3]. Under the effect of the self-adjusting, the synchronous velocity of two motors is about 1560 r/min. After about 20 s, motor 2 begins to execute the control command and track the phase of motor 1. According to the results of Figure 9, motor 1 is the lagging phase ER affected by the self-adjusting. To achieve the synchronous motion of two motors with the zero phase difference, the motion tendency of motor 2 should wait for the tracking of motor 1. The synchronous velocity of two motors rapidly decreases to about 1420 r/min when motor 2 is acted by phase control, and the velocity difference is about 140 r/min. After 40 s, because motor 1 is controlled to track the phase of motor 2, the synchronous velocity of two motors rapidly increases to about 1670 r/min. For the 2nd exchange between the master motor and the slave motor, there is a maximum value in the velocity curves because of the quick switch. This above phenomenon reflects the dynamic characteristic of the vibration system.

Figure 10(b) shows the phase difference curve between two ERs. From the results of Figures 8 and 10(a), when two motors run in the state of vibration synchronization, the phase difference is close to −170°. However, when the command of control synchronization is executed, the stable phase difference in the 2nd stage is close to 0°. Because the absolute value of the phase difference in the 1st stage is close to 180°, the phase controller encounters with multiple judgment results of Figure 4, which results in a chattering phenomenon acting by DSMC. This experiment proves the feasibility of the control scheme of controlling only one motor in the vibration system. In order to verify the robust of the phase controller, the master motor and the slave motor are exchanged after 40 s, which still selects this control scheme. Except for the change in the velocity curves of Figure 10(a), there is no change in the phase curves of Figure 10(b) and the phase difference is still equal to zero in the steady state. Of course, there is still a fluctuation at the moment of the command switching. The data correctness of Figure 10(b) is verified according to the eight photos in Figure 9.

Figures 10(c) and 10(d) are the amplitudes of the mass center in both x and y directions. Similarly, Figures 10(e) and 10(f) are the amplitudes of the body edge. Comparing two measuring positions, the amplitude of y_1 is much bigger than those of x_0, y_0, and x_1 when the vibration system operates in the state of vibration synchronization. However, the amplitude of y_1 is the smallest in these amplitudes when the vibration system operates in the state of control synchronization. Obviously, the amplitudes of the 2nd control synchronization are bigger than those of the 1st control synchronization because of the different synchronous velocity. In order to directly compare the motions of two positions, the motion trajectory is shown in Figures 10(g) and 10(h). Three domains of inclined ellipse trajectory indicate clearly that the motion of the vibration system in the state of control synchronization is the ideal trajectory. These motion laws are in accordance with the motion pattern of a rigid body under the different resultant forces.

From the experimental results in Figure 10, the phase controller can be adopted on the arbitrary slave motor to achieve the synchronous motion of two ERs with the zero phase difference, which also proves the effectiveness of the proposed phase controller. The acceleration amplitude of the vibration system is affected by the synchronous velocity due to tracking of different slave motors.. These results of control synchronization show that the vibration system has achieved the ideal motion trajectory and the maximum force with the

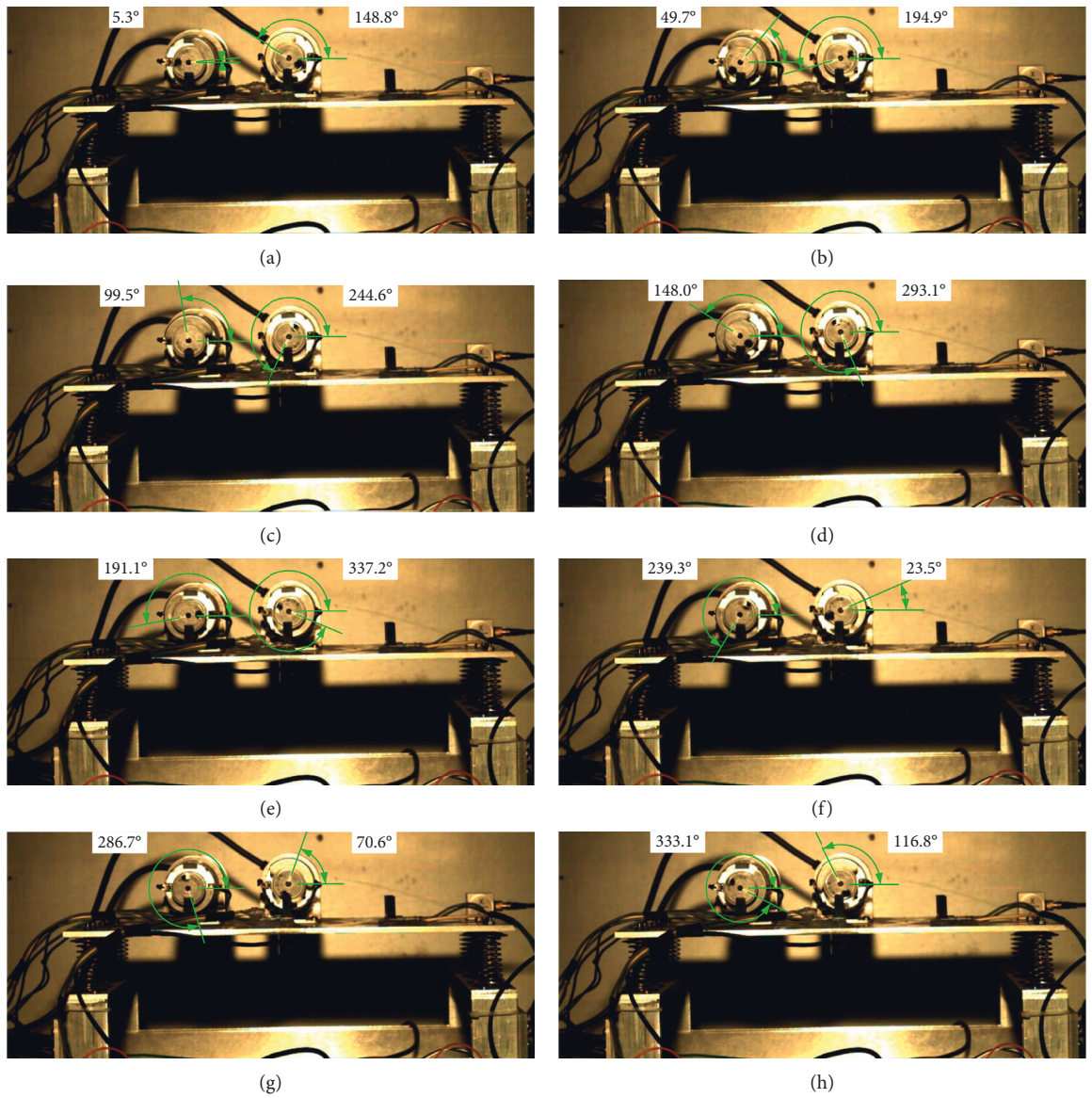

FIGURE 7: The phase difference of vibration synchronization of two ERs with the anticlockwise rotational direction. (a) $\varphi_1 - \varphi_2 \approx -143.5^\circ$, (b) $\varphi_1 - \varphi_2 \approx -145.2^\circ$, (c) $\varphi_1 - \varphi_2 \approx -145.1^\circ$, (d) $\varphi_1 - \varphi_2 \approx -145.1^\circ$, (e) $\varphi_1 - \varphi_2 \approx -146.1^\circ$, (f) $\varphi_1 - \varphi_2 \approx -144.2^\circ$, (g) $\varphi_1 - \varphi_2 \approx -143.9^\circ$, and (h) $\varphi_1 - \varphi_2 \approx -143.7^\circ$.

scheme of controlling one motor. Therefore, it is a very engineering technology that applies the technology of control synchronization to replace vibration synchronization in the design of a vibration machine.

5.2. Control Synchronization of Controlling One Motor and Two Motors. Figure 11 shows the comparison of controlling one motor and two motors, which is used to further verify the feasibility of control synchronization. The experiment is also divided into three stages, and motor 1 is chosen as the slave motor and motor 2 is chosen as the master motor. In the 1st stage, motor 2 adopts the open-loop control. In the 2nd stage, motor 2 adopts the closed-loop control with the velocity controller. In the 3rd stage, motor 2 still adopts the velocity controller, and the velocity goal of motor 2 is set smaller than that of the 2nd case.

The velocity curves of two motors are shown in Figure 11(a), and they are similar to Figure 10(a). However, there is a different phenomenon that the velocities of two motors appear overshoot at the ascending stage with the control of the phase controller. Since the master motor adopts the open-loop control and it is tracked by the slave motor, the load torque of the master motor is reduced, resulting in increasing its velocity, which is the result of load distribution with the self-adjusting. In the 2nd stage, the synchronous velocity is stable at about 1670 r/min. Comparing with Figure 10(a), although there are some fluctuations at the beginning of the 2nd stage, it does not explain that the velocity controller is not stable enough but the limitation of calculating velocity signal. Because the method

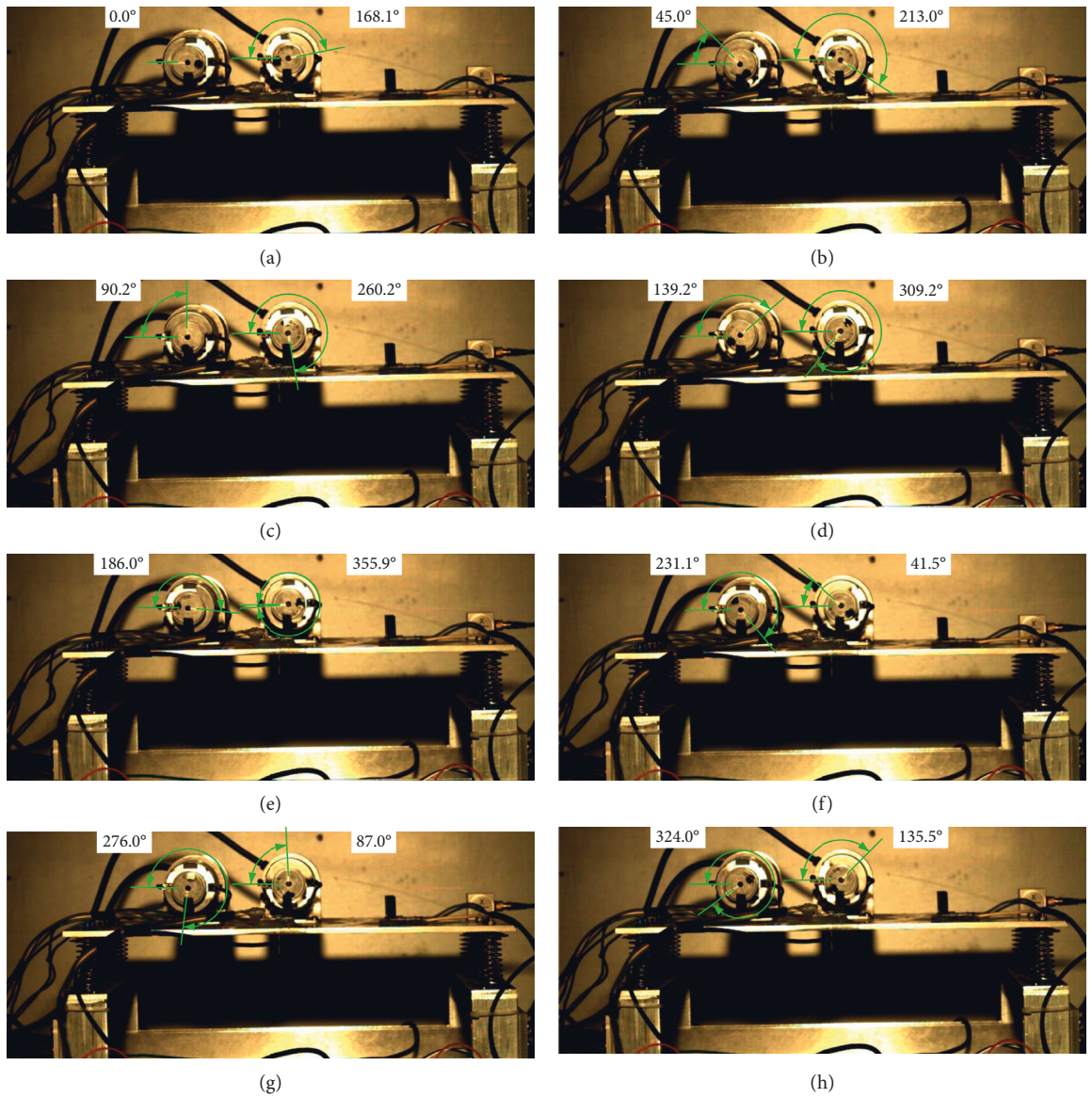

FIGURE 8: The phase difference of vibration synchronization of two ERs with the clockwise rotational direction. (a) $\varphi_1 - \varphi_2 \approx -168.1^\circ$, (b) $\varphi_1 - \varphi_2 \approx -168^\circ$, (c) $\varphi_1 - \varphi_2 \approx -170.1^\circ$, (d) $\varphi_1 - \varphi_2 \approx -170^\circ$, (e) $\varphi_1 - \varphi_2 \approx -166.9^\circ$, (f) $\varphi_1 - \varphi_2 \approx -170.4^\circ$, (g) $\varphi_1 - \varphi_2 \approx -171^\circ$, and (h) $\varphi_1 - \varphi_2 \approx -171.5^\circ$.

of the calculating velocity in Section 4.2 needs multiple motor rotational periods to guarantee the accuracy of the velocity value, which affects the timeliness of the velocity control. In the 2nd stage, the goal value is set as 1700 r/min to verify the effectiveness of the velocity controller, which is higher than the value in the 1st stage. After motor 2 operates with the velocity control, the synchronous velocity of two motors rises slowly and finally stabilizes around 1700 r/min, and the synchronous velocity increases by about 30 r/min. In order to verify the robustness of the velocity controller, the goal value is set as 1620 r/min. After the velocity adjustment of several seconds, the synchronous velocity of two motors stabilizes around 1620 r/min.

Similarly, Figure 11(b) shows the phase difference between two ERs. The phase difference remains near 0° for all the time except in two switching stages where it fluctuates. The reason for the phase difference fluctuating at the beginning of the 1st stage is the same as Figure 10(b), which affected by the phase controller. However, the reason for the phase difference fluctuating at the beginning of the 2nd stage and the 3rd stage is affected by the velocity controller.

Comparing the amplitudes of two positions in Figures 11(c) to 11(f), it can be seen that the amplitudes of x direction are greater than those of y direction, and the phase angles of x direction are lag of those of y direction, which explains that the motion trajectory is an inclined ellipse. They also are shown in Figures 11(g) and 11(h). From those, it can be concluded that the motion trajectory of different positions is changing with the distance between it and the excitation resource, which conforms to the dynamic characteristic with the eccentric excitation.

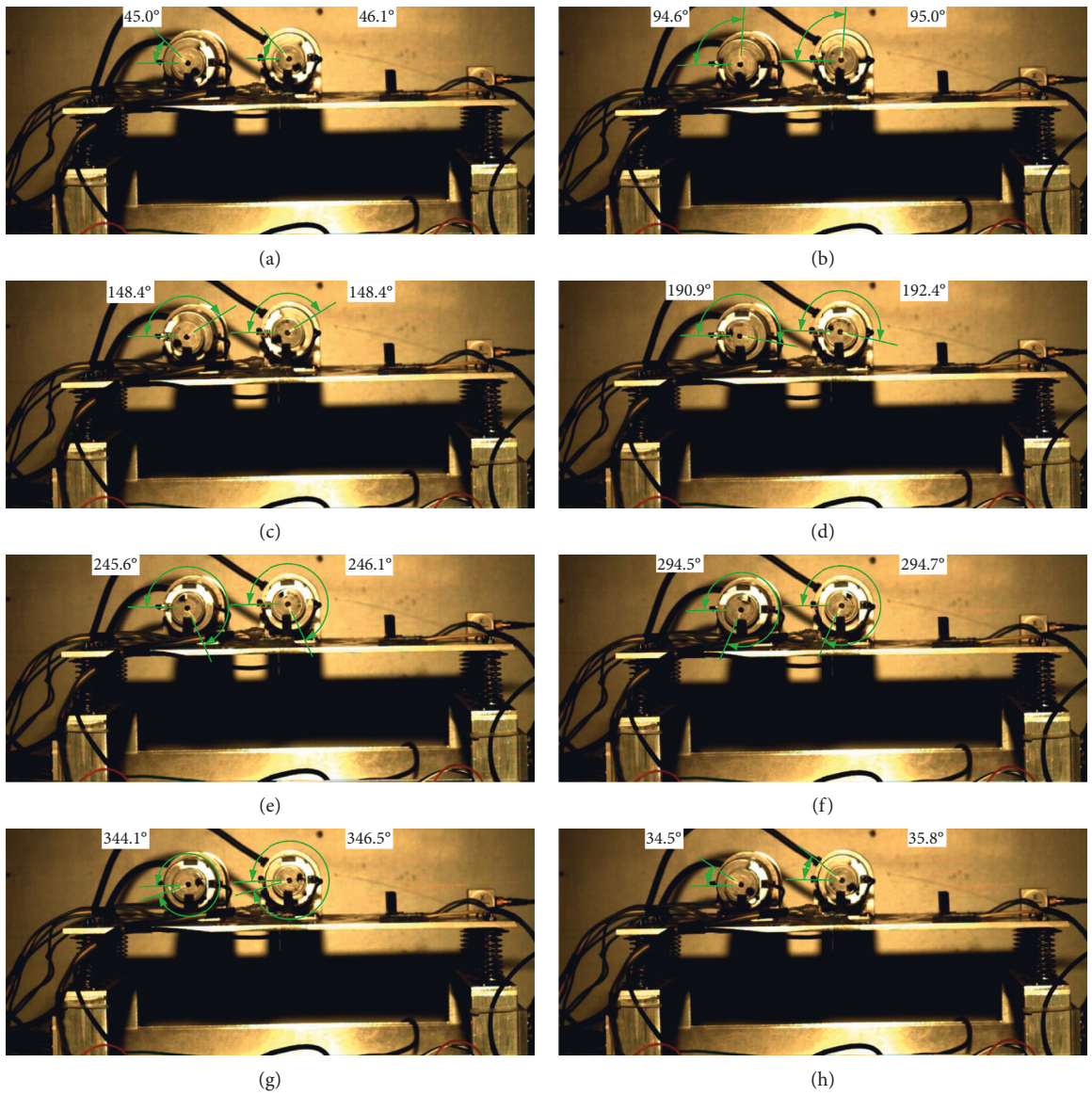

Figure 9: The phase difference of the control synchronization of two ERs with the clockwise rotational direction. (a) $\varphi_1 - \varphi_2 \approx 0^\circ$, (b) $\varphi_1 - \varphi_2 \approx -0.3^\circ$, (c) $\varphi_1 - \varphi_2 \approx -0.1^\circ$, (d) $\varphi_1 - \varphi_2 \approx 0.5^\circ$, (e) $\varphi_1 - \varphi_2 \approx -0.5^\circ$, (f) $\varphi_1 - \varphi_2 \approx -1.3^\circ$, (g) $\varphi_1 - \varphi_2 \approx -0.9^\circ$, and (h) $\varphi_1 - \varphi_2 \approx 0.7^\circ$.

According to the experimental analysis in Figure 11, the conclusion is drawn that the zero-phase difference motion of two ERs in the vibration system can be achieved by controlling one motor, but the synchronization velocity is not guaranteed because of the self-adjusting. Only the master motor using the velocity control can achieve the ideal synchronous motion of two ERs in the vibration system. In this experiment, because the slave motor is controlled by the phase controller at the beginning, the fluctuations of the velocity curves and the phase difference are more obvious than those in the state of vibration synchronization in Figure 10. Because the interference comes from the self-adjusting of the vibration system and its changes are consistent with the input of controllers, it reflects the control complexity of the vibration system.

From the above two experiments, we can see that the vibration system has the ability of self-adjusting, which depends on the coupling of the electromechanical system. The motor drives ER to excite the mechanical system. Meanwhile, the mechanical system exerts the load torque on the motor through the coupling motion between the vibration body and ER, which is manifested as the change of the motor velocity and the phase of ER [29]. The self-adjusting ability of the vibration system can be regarded as a closed-loop control. Its control goal is to make the mechanical system satisfy the minimum potential energy principle, that is, the motion of the mass center of the mechanical system tends to be motionless [15, 16]. When we introduce the control system into the vibration system, the overall system has two sets of control systems. However, the control goals of the two control systems are exactly the opposite. These reasons make control synchronization difficult. When changing operating conditions in our experiments, such as changing the motor speed, control

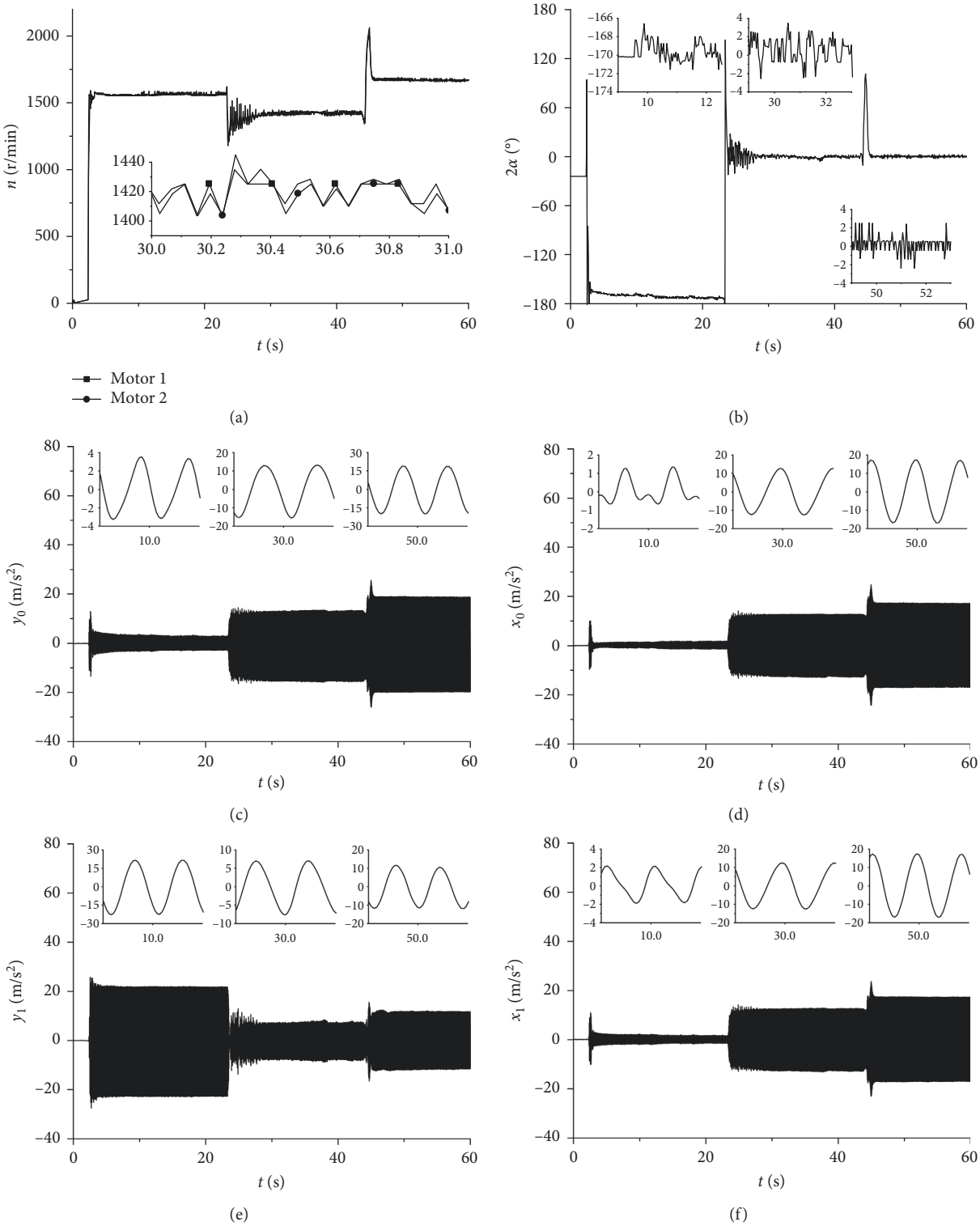

Figure 10: Continued.

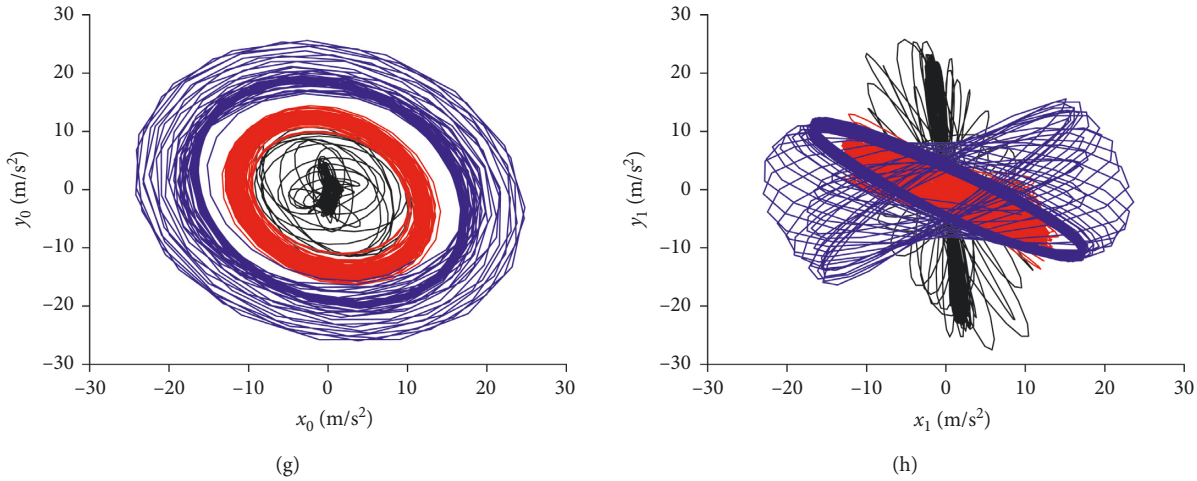

Figure 10: Comparing vibration synchronization and control synchronization. (a) The velocities of two motors. (b) The phase difference. (c) Amplitude of the mass center in y-direction. (d) Amplitude of the mass center in x-direction. (e) Amplitude of the edge position in y-direction. (f) Amplitude of the edge position in x-direction. (g) Mass center trajectory. (h) Edge position trajectory.

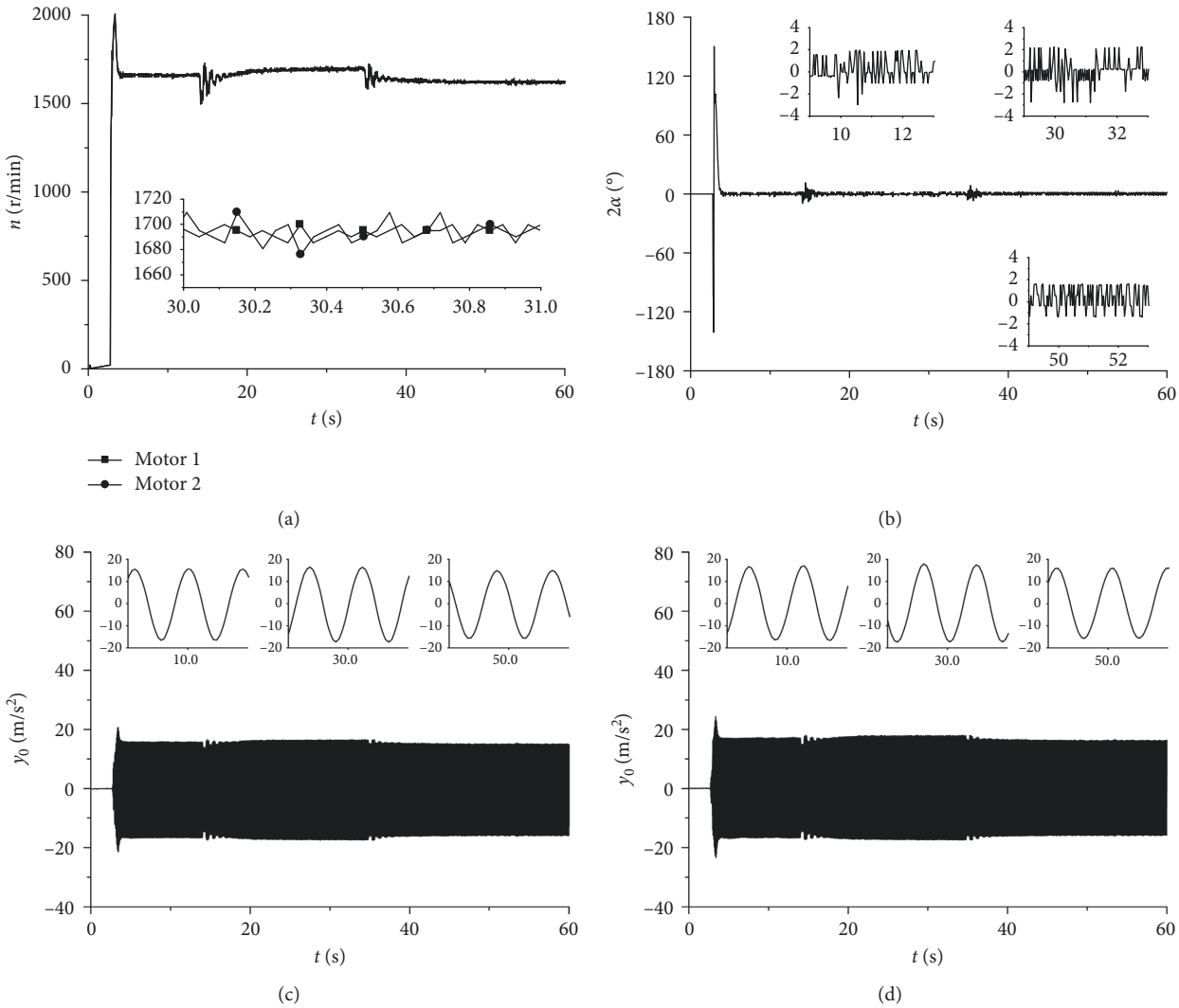

Figure 11: Continued.

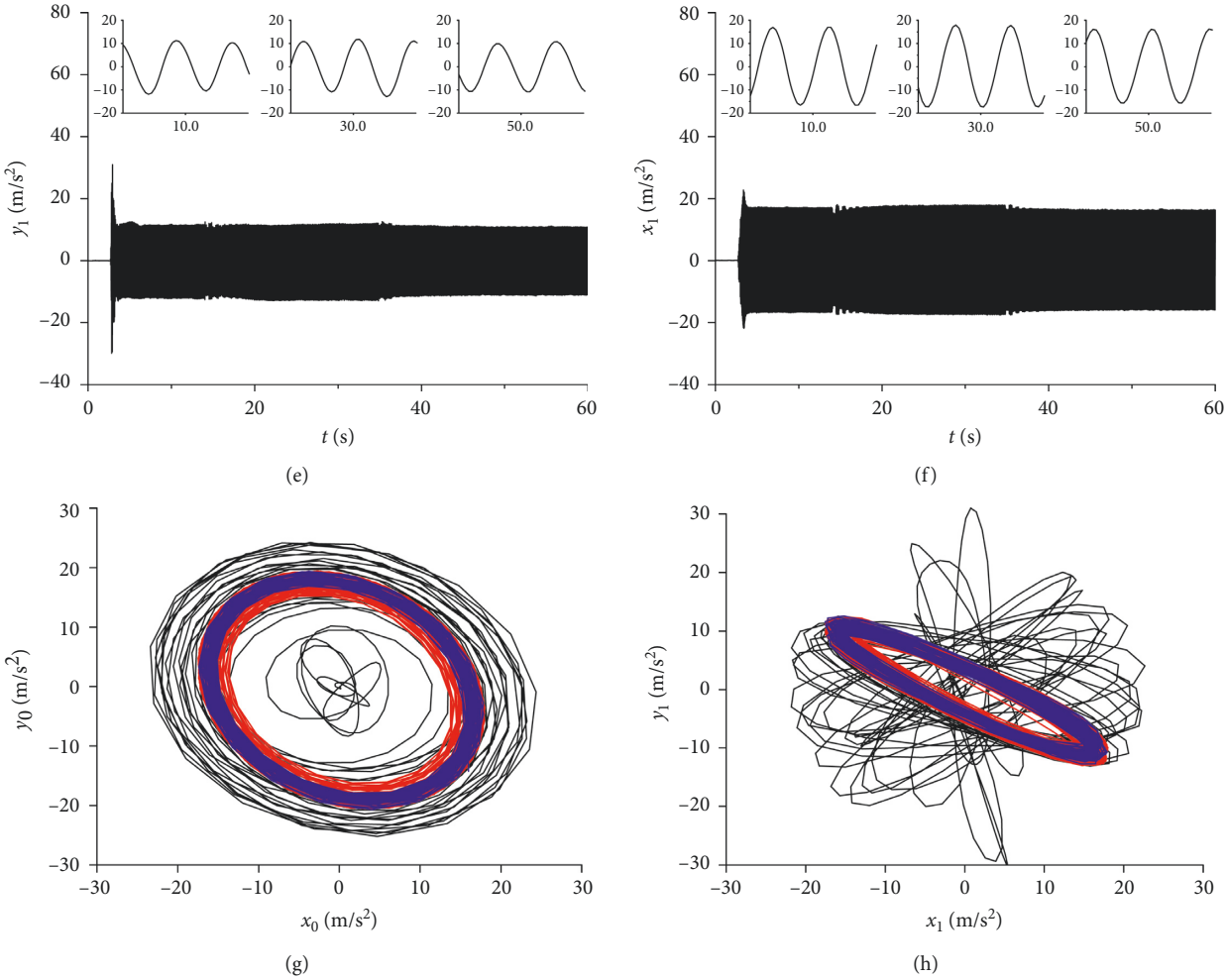

Figure 11: Comparing control synchronization of controlling one motor and two motors. (a) The velocities of two motors. (b) The phase difference. (c) Amplitude of the mass center in y-direction. (d) Amplitude of the mass center in x-direction. (e) Amplitude of the edge position in y-direction. (f) Amplitude of the edge position in x-direction. (g) Mass center trajectory. (h) Edge position trajectory.

synchronization becomes more complicated. According to the coupling dynamics characteristics of the vibration system, when the motor velocity is increased, the coupling strength of the vibration system is actually enhanced and the self-adjusting ability of the vibration system is increased [3, 4]. From the control perspective, the enhanced self-adjusting ability of the vibration system leads to an increase of interference for the control system. Therefore, the instantaneous change of the motor velocity increases the control error. Based on our experimental results, SMC is a good choice for this kind of the large disturbance working condition.

6. Conclusions

In order to remove the limitation of vibration synchronization, control synchronization of two ERs in the vibration system with the asymmetric structure is investigated in this paper. By introducing the master-slave control scheme, the motion requirements of the vibration system are converted into the velocity and the phase tracking between two motors. Considering the engineering application, velocity and phase controllers are designed by employing DSMC. The performance of the proposed controllers is evaluated by experiments of a vibration machine driven by two DC vibration motors. The following remarks should be stressed:

(1) Because the goal of control synchronization is the same phase motion of two motors, it is necessary to estimate the phase difference between two motors because it determinates which motor is the leading phase and provides the tracking data for the controller. The phase difference in the vibration system is expressed to be less than π, which is more convenient for the controller. Therefore, from the aspect of the signal acquisition, a matching method dividing the pulses of two encoders into four quadrants in Figure 4 is proposed for this purpose.

(2) In order to better analyze the motion characteristics of the vibration system under the control synchronization state, the experiment is divided into

three cases: vibration synchronization, control of one motor, and control of two motors at the same time. Comparing the experimental results of three cases in Figures 10 and 11, the master-slave control is a simple and cost-saving control scheme for engineering because it can achieve the synchronous motion of 0° phase difference of two motors although the phase difference is close to −170° under the vibration synchronization state. However, the synchronous velocity of two motors with controlling only one motor will change with the self-adjusting of the vibration system in Figure 10. Of course, this phenomenon does not appear in the master motor adopting the velocity controller in Figure 11.

(3) Because the vibration system has the self-adjusting function, the phase of the left motor is lag of that of the right motor with the asymmetric structure under the vibration synchronization state in Figure 7 (the phase difference is basically stable at −145° with the anticlockwise) and Figure 8 (the phase difference is basically stable at −170° with the clockwise). When master motor adopts the open-looped control and operates in the clockwise, if the right motor is the master one, the synchronous velocity will rise about 110 r/min because of the tracking of the left motor. On the contrary, if the left motor is the master one, the synchronous velocity will drop about 140 r/min because the right motor is waiting for the left motor.

(4) From Figures 10(g), 10(h), 11(g), and 11(h), it can be concluded that the motion trajectory of different position is changing with the distance between it and the excited resource when the vibration system operates with control synchronization. Hence, the design of vibration machines requiring eccentric excitation should introduce the method of control synchronization to replace the method of forced synchronization.

Data Availability

The data used to support the findings of this study are available from the corresponding author upon request.

Conflicts of Interest

The authors declared no potential conflicts of interest with respect to the research, authorship, and/or publication of this article.

Acknowledgments

This work was supported by the Fundamental Research Funds for the Central Universities (N172303011) and Key Laboratory of Vibration and Control of Aero-Propulsion System Ministry of Education, Northeastern University (VCAME201704).

References

[1] B. C. Wen, H. Zhang, and S. Y. liu, *Theory and Techniques of Vibrating Machinery and their Applications*, Science Press, Beijing, China, 2010.

[2] C. Zhao, H. Zhu, R. Wang, and B. Wen, "Synchronization of two non-identical coupled exciters in a non-resonant vibrating system of linear motion. Part I: theoretical analysis," *Shock and Vibration*, vol. 16, no. 5, pp. 505–515, 2009.

[3] X.-L. Zhang, C.-Y. Zhao, and B.-C. Wen, "Theoretical and experimental study on synchronization of the two homodromy exciters in a non-resonant vibrating system," *Shock and Vibration*, vol. 20, no. 2, pp. 327–340, 2013.

[4] X. Chen, X. Kong, X. Zhang, L. Li, and B. Wen, "On the synchronization of two eccentric rotors with common rotational Axis: theory and experiment," *Shock and Vibration*, vol. 2016, Article ID 6973597, 14 pages, 2016.

[5] I. I. Blekhman, A. L. Fradkov, H. Nijmeijer, and A. Y. Pogromsky, "On self-synchronization and controlled synchronization," *Systems & Control Letters*, vol. 31, no. 5, pp. 299–305, 1997.

[6] I. I. Blekhman, A. L. Fradkov, O. P. Tomchina, and D. E. Bogdanov, "Self-synchronization and controlled synchronization: general definition and example design," *Mathematics and Computers in Simulation*, vol. 58, no. 4-6, pp. 367–384, 2002.

[7] J. M. Balthazar, J. L. P. Felix, and R. M. L. R. F. Brasil, "Short comments on self-synchronization of two non-ideal sources supported by a flexible portal frame structure," *Modal Analysis*, vol. 10, no. 12, pp. 1739–1748, 2004.

[8] A. A. N. Djanan and B. R. N. Nbendjo, "Effect of two moving non-ideal sources on the dynamic of a rectangular plate," *Nonlinear Dynamics*, vol. 92, no. 2, pp. 645–657, 2018.

[9] E. Kibirkstis, D. Pauliukaitis, V. Miliunas, and K. Ragulskis, "Synchronization of pneumatic vibroexciters operating on air cushion with feeding pulsatile pressure under autovibration regime," *Journal of Mechanical Science and Technology*, vol. 32, no. 1, pp. 81–89, 2018.

[10] P. Koluda, P. Perlikowski, K. Czolczynski, and T. Kapitaniak, "Synchronization of two self-excited double pendula," *European Physical Journal Special Topics*, vol. 223, no. 4, pp. 613–629, 2014.

[11] Á. Miklós and Z. Szabó, "Simulation and experimental validation of the dynamical model of a dual-rotor vibrotactor," *Journal of Sound and Vibration*, vol. 334, pp. 98–107, 2015.

[12] D. Sado, "Nonlinear dynamics of a non-ideal autoparametric system with MR damper," *Shock and Vibration*, vol. 20, no. 6, pp. 1065–1072, 2013.

[13] P. Fang, Y. Hou, L. Dai, and M. Du, "Theoretical study of synchronous behavior in a dual-pendulum-rotor system," *Shock and Vibration*, vol. 2018, Article ID 9824631, 13 pages, 2018.

[14] D. Dudkowski, K. Czołczyński, and T. Kapitaniak, "Synchronization of two self-excited pendula: influence of coupling structure's parameters," *Mechanical Systems and Signal Processing*, vol. 112, pp. 1–9, 2018.

[15] X. Zhang, C. Li, Z. Wang, and S. Cui, "Synchronous stability of four homodromy vibrators in a vibrating system with double resonant types," *Shock and Vibration*, vol. 2018, Article ID 9641231, 20 pages, 2018.

[16] X. Zhang, B. Wen, and C. Zhao, "Vibratory synchronization and coupling dynamic characteristics of multiple unbalanced rotors on a mass-spring rigid base," *International Journal of Non-Linear Mechanics*, vol. 60, pp. 1–8, 2014.

[17] X. Kong, X. Chen, J. Dou, X. Zhang, and B. Wen, "Controlled synchronization of two nonidentical homodromy coupling exciters driven by inductor motors in a vibratory system," *Proceedings of the Institution of Mechanical Engineers, Part C: Journal of Mechanical Engineering Science*, vol. 230, no. 17, pp. 3040–3054, 2016.

[18] B. Sencer, T. Mori, and E. Shamoto, "Design and application of a sliding mode controller for accurate motion synchronization of dual servo systems," *Control Engineering Practice*, vol. 21, no. 11, pp. 1519–1530, 2013.

[19] C.-S. Chen and L.-Y. Chen, "Robust cross-coupling synchronous control by shaping position commands in multiaxes system," *IEEE Transactions on Industrial Electronics*, vol. 59, no. 12, pp. 4761–4773, 2012.

[20] S. Lin, Y. Cai, B. Yang, and W. Zhang, "Electrical line-shafting control for motor speed synchronisation using sliding mode controller and disturbance observer," *IET Control Theory & Applications*, vol. 11, no. 2, pp. 205–212, 2017.

[21] L.-B. Li, L.-L. Sun, S.-Z. Zhang, and Q.-Q. Yang, "Speed tracking and synchronization of multiple motors using ring coupling control and adaptive sliding mode control," *ISA Transactions*, vol. 58, pp. 635–649, 2015.

[22] O. Tomchina and I. Kudryavtseva, "Controlled synchronization of unbalanced rotors with flexible shafts in time-varying vibrational units," in *Proceedings-IEEE 2005 International Conference Physics and Control*, pp. 790–794, Saint Petersburg, Russia, August 2005.

[23] L. Jia, X. Kong, J. Zhang, Y. Liu, and B. Wen, "Multiple-frequency controlled synchronization of two homodromy eccentric rotors in a vibratory system," *Shock and Vibration*, vol. 2018, Article ID 4941357, 12 pages, 2018.

[24] A. Fradkov, O. Galitskaya, and D. Gorlatov, "Multiple controlled synchronization for 3-rotor vibration unit with varying payload," *IFAC Proceedings Volumes*, vol. 46, no. 12, pp. 5–10, 2013.

[25] Y. Eun, J. H. Kim, K. Kim, and D. I. Cho, "Discrete-time variable structure controller with a decoupled disturbance compensator and its application to a CNC servomechanism," *IEEE Transactions on Control Systems Technology*, vol. 7, no. 4, pp. 414–423, 1999.

[26] W. B. Gao, Y. F. Wang, and A. Homaifa, "Discrete-time variable-structure control-systems," *IEEE Transactions on Industrial Electronics*, vol. 42, no. 2, pp. 117–122, 1995.

[27] C.-W. Chuang, C.-L. Haung, C.-D. Lee, C.-C. Kao, and R.-F. Fung, "Synchronization and tension control of dual motor systems via MIMO discrete pseudo model following integral variable structure control," *Mechanism and Machine Theory*, vol. 44, no. 2, pp. 499–510, 2009.

[28] Z. Deng, J. Shang, and X. Nian, "Synchronization controller design of two coupling permanent magnet synchronous motors system with nonlinear constraints," *ISA Transactions*, vol. 59, pp. 243–255, 2015.

[29] X. Chen, X. Kong, J. Dou, Y. Liu, and B. Wen, "Numerical and experimental investigation on self-synchronization of two eccentric rotors in the vibration system," *Journal of Vibroengineering*, vol. 18, no. 2, pp. 744–758, 2016.

[30] X. Wang and C. S. Suh, "Precision concurrent speed and position tracking of brushed dc motors using nonlinear time-frequency control," *Journal of Vibration and Control*, vol. 23, no. 19, pp. 3266–3291, 2017.

[31] V. Utkin, J. Guldner, and J. X. Shi, *Sliding Mode Control in Electro-Mechanical Systems*, CRC Press, NewYork, NY, USA, 2009.